nature COMMUNICATIONS

ARTICLE

Received 29 May 2015 | Accepted 28 Jul 2015 | Published 1 Sep 2015

DOI: 10.1038/ncomms9197 OPEN

Settling time of a vibrational wavepacket in ionization

Yasuo Nabekawa[1], Yusuke Furukawa[1], Tomoya Okino[1], A. Amani Eilanlou[1], Eiji J. Takahashi[1], Kaoru Yamanouchi[2] & Katsumi Midorikawa[1]

The vibrational wavepacket of a diatomic molecular ion at the time of ionization is usually considered to be generated on the basis of the Franck–Condon principle. According to this principle, the amplitude of each vibrational wavefunction in the wavepacket is given by the overlap integral between each vibrational wavefunction and the ground vibrational wavefunction in the neutral molecule, and hence, the amplitude should be a real number, or equivalently, a complex number the phase of which is equal to zero. Here we report the observation of a non-trivial phase modulation of the amplitudes of vibrational wavefunctions in a wavepacket generated in the ground electronic state of a H_2^+ molecular ion at the time of ionization. The phase modulation results in a group delay of the specific vibrational states of order 1 fs, which can be regarded as the settling time required to compose the initial vibrational wavepacket.

[1] Attosecond Science Research Team, RIKEN Center for Advanced Photonics (RAP), 2-1 Hirosawa, Wako-shi, Saitama 351-0198, Japan. [2] Department of Chemistry, School of Science, The University of Tokyo, 7-3-1 Hongo, Bunkyo, Tokyo 113-0033, Japan. Correspondence and requests for materials should be addressed to Y.N. (email: nabekawa@riken.jp).

The H_2^+ molecular ion has been widely investigated to obtain essential benchmarks in molecular physics because it has the simplest structure among molecules. The real-time observations of a vibrational wavepacket of H_2^+ using an a-few-cycle laser pulse[1,2], an attosecond high-harmonic pulse[3], and an X-ray free-electron laser pulse[4] are examples of such fundamental studies. In these studies, a vibrational wavepacket in the ground bound state ($1s\sigma_g$) of H_2^+ is created by the ionization of H_2 with a pump pulse. Then, after a time delay, the H_2^+ is excited to the repulsive state of H_2^+ or further ionized into the doubly charged state by the irradiation of a second probe pulse. The real-time motion of the wavepacket can be tracked by measuring the ion fragments of H^+ or detached electrons by scanning the delay of the probe pulse.

In general, a vibrational wavepacket in the $1s\sigma_g$ state of H_2^+ at time t, $\varphi^g(R;t)$, is expressed as a coherent superposition of vibrational wavefunctions, $\chi_v^g(R)$, with the time-evolving phase factor of $e^{-i\omega_v^g t}$, namely, $\varphi^g(R;t) = \sum_v a_v \chi_v^g(R)\, e^{-i\omega_v^g t}$ (ref. 2), where v is the vibrational quantum number and the internuclear distance and the amplitude of the vth vibrational wavefunction are denoted as R and a_v, respectively. The eigenenergy of the vth vibrational state coincides with $\hbar\omega_v^g$. The constant of proportionality, $\hbar$, is Planck's constant divided by 2π. Although the amplitude, a_v, can generally be a complex number[1,5], we commonly substitute a_v^{fc} for a_v as a good approximation for the situation of an ultrafast ionization process, where a_v^{fc} is obtained from an overlap integral of $\chi_v^g(R)$ and $\chi_0^X(R)$ as $a_v^{fc} = \int_0^\infty dR \chi_v^g(R)\chi_0^X(R)$, where $\chi_0^X(R)$ is the ground vibrational wavefunction in the $X^1\Sigma_g^+$ state of a neutral H_2 molecule. A detailed theoretical model considering the electronic transition moment can provide us with a more accurate a_v, and then, the resultant magnitude correction for a_v can be used to prove the consistency of the experimental data[6]. Magnitude correction is also necessary when H_2^+ is generated via tunnelling ionization with an intense near-infrared laser pulse[5,7]. In contrast, the phase of a_v at ionization has been omitted, or at least, it has not yet been necessary to consider it to explain the experimental data related to the ionization of H_2.

In this paper, we demonstrate a non-trivial phase modulation of a_v, measured by applying the frequency-resolved optical gating (FROG)[8] technique to the two-dimensional delay-energy spectrogram of H^+ fragment ions[9]. This is the first measurement, to the best of our knowledge, of the phase at the time of birth of a vibrational wavepacket. We have found that the phase modulation is caused by the interference of the phase in the wavefunction of a continuum electron ionized by the one-photon absorption of an extreme ultraviolet (XUV) attosecond pulse train (APT).

Results

Experimental data. We show a schematic of the energy diagram for the generation and observation of the H_2^+ (or D_2^+) vibrational wavepacket adopted in our experiment in Fig. 1. The spectrum of an APT[10,11] used to ionize H_2 is shown in Supplementary Fig. 1. In our experiment, a vibrational wavepacket in the $1s\sigma_g$ state is first created via the ionization of H_2 by absorbing one photon in a pump pulse composed of the harmonic spectrum ranging from the 11th to 21st orders. Then, the H_2^+ molecule dissociates by excitation from the $1s\sigma_g$ state to the repulsive $2p\sigma_u$ state by the absorption of another photon in the probe pulse accompanying the 3rd and 5th components (represented as light blue and violet arrows in Fig. 1, respectively), resulting in the kinetic energy release (KER) spectrum of H^+ fragments exhibiting two peaks at $\sim$3 and $\sim$5.7 eV, shown as a light brown curve with a shaded area on the right-hand side of Fig. 1. Another peak at $\sim$0.8 eV is ascribed to the excitation by absorbing the fundamental photon. We obtained the two-dimensional spectrogram of H^+ fragments shown in Fig. 2a by scanning the delay of the probe pulse. The experimental[12,13] detail and the reason why we disregard the KER spectrum at low KER region are described in Supplementary Note 1.

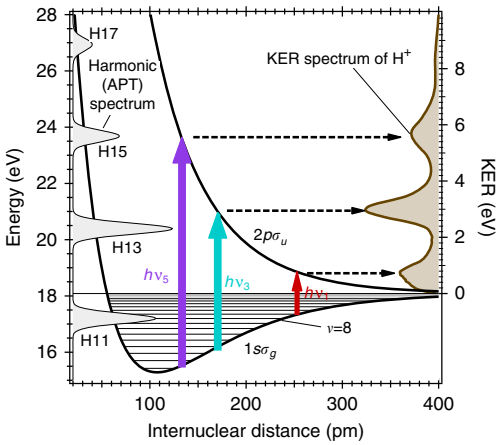

Figure 1 | Experimental scheme. The relevant adiabatic potential energy curves ($1s\sigma_g$ and $2p\sigma_u$) of H_2^+ are shown as solid black curves. A typical KER spectrum of a H^+ ion is depicted as a brown curve with a shaded area on the right-hand side. The harmonic spectrum ranging from the 11th to 17th orders in the pump APT to ionize neutral H_2 is shown as a grey curve with shaded areas. The energy on the left axis, indicating the photon energy of the high-harmonic and the energy of the adiabatic potential, is measured from the ground vibrational state of the $X^1\Sigma_g^+$ electronic state of H_2. The vibrational wavepacket created in the $1s\sigma_g$ state is probed by one-photon excitation to the $2p\sigma_u$ state by absorbing the 3rd- and 5th-order harmonic components in the probe APT, which are indicated by light blue and violet arrows, respectively. The weak fundamental component, depicted as a red arrow, also excites the $1s\sigma_g$ state, while this component was not used to retrieve the vibrational wavepacket amplitude.

Phase retrieval of vibrational wavefunction. The first aim of our study is to extract the phase factor from the measured delay-KER spectrogram in Fig. 2a. Thus, we adopted a physical model that suitably expresses the excitation process from the $1s\sigma_g$ to $2p\sigma_u$ states, which is based on the Hamiltonian of a two-level system interacting with an optical field via a dipole interaction[2,5,14]. This kind of Hamiltonian is widely used for analysing the vibrational wavepacket dynamics of a H_2^+ molecular ion. By applying time-dependent perturbation theory to the Schrödinger equation with this Hamiltonian, we found the one-photon transition amplitude from the $1s\sigma_g$ to $2p\sigma_u$ states to be

$$T(\omega^u;\tau) \propto \sum_v \mathscr{M}\left(\omega^u;\omega_v^g\right)\tilde{G}\left(\omega^u-\omega_v^g\right)a_v e^{-i\omega_v^g\tau}. \qquad (1)$$

The derivation of this equation is presented in ref. 9. We also briefly describe the theoretical model used to obtain this equation in Supplementary Note 2.

On the right-hand side of equation (1), the wavepacket amplitude, a_v, is convolved with the positive-frequency part of the Fourier amplitude of the probe optical field (an optical field composed of the coherent superposition of the 3rd- and 5th-order harmonic fields in the actual experiment), $\tilde{G}(\Omega)$, with a delay-dependent phase factor, $e^{-i\omega_v^g\tau}$, and then mapped onto the repulsive state via the matrix elements of the electronic transition dipole moment, $\mathscr{M}(\omega^u;\omega_v^g) \equiv \int_0^\infty dR\chi^u(\omega^u;R)\mu(R)\chi_v^g(R)$. The nuclear wavefunction in the $2p\sigma_u$ state with an eigenenergy of

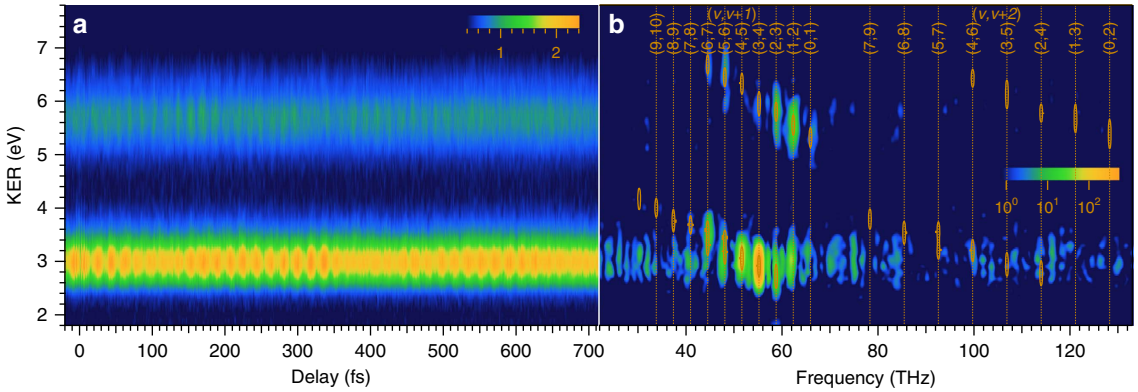

Figure 2 | Experimental result. (**a**) Delay-KER spectrogram of H^+ fragments measured using a velocity mapping imaging (VMI) spectrometer. (**b**) Magnitude square of the Fourier transform of the delay-KER spectrogram in Fig. 2a. The color scale in (**a**) changes linearly with the intensity, while a logarithmic scale is used to plot the intensity in (**b**) to clearly exhibit the beat frequency components. Pairs of numbers assigning vibrational states as beat frequency sources are depicted at the top of this figure. We also depict the bandpass filter used to obtain the target delay-KER spectrogram, shown in Fig. 3a, as contour plots (ellipses).

$\hbar\omega^u$ and the electronic transition dipole moment are defined as $\chi^u(\omega^u;R)$ and $\mu(R)$, respectively.

Note that equation (1) is only valid under the condition that the probe pulse does not temporally overlap with the pump pulse (XUV APT) used for ionization. The magnitude square of $T(\omega^u;\tau)$ should be proportional to the delay-KER spectrogram of H^+. As a result, we noticed that this spectrogram is very similar to that obtained when using the FROG technique to characterize the magnitude and phase of an ultrashort optical pulse. A detailed discussion of this similarity is given in ref. 9 and in Supplementary Note 2.

We have developed an iterative algorithm based on the generalized projection method in accordance with equation (1), which we call the matter-wave FROG (MW-FROG) algorithm hereafter. Note that we need a priori knowledge of the nuclear wavefunctions $\chi^u(\omega^u;R)$ and $\chi^g_v(R)$ and of the dipole moment $\mu(R)$ to specify $\mathscr{M}(\omega^u;\omega^g_v)$. Therefore, we used the adiabatic potentials of the $1s\sigma_g$ and $2p\sigma_u$ states obtained from theoretical calculations[15] to determine $\chi^u(\omega^u;R)$ and $\chi^g_v(R)$. The dipole moment is assumed to be a real number and proportional to R[16].

Application of MW-FROG. Before implementing the MW-FROG algorithm, we need to adapt the measured spectrogram to obtain an appropriate target spectrogram. Because the phase information of the vibrational states is only contained in the beat frequency components $\omega^g_v-\omega^g_{v'}$ $(v\neq v')$, we apply a bandpass filter to the measured spectrogram to remove the frequency components irrelevant to the vibrational states, as shown in Fig. 2b. The magnitude square of the Fourier transform of the measured spectrogram clearly exhibits the beat frequencies with $v-v'=1$ and 2 as distinct peaks in this figure. The vibrational quantum numbers that we can specify from the experimental data are limited to <9, hence we restrict the range of v to 0–8 in the MW-FROG algorithm. We extracted these frequency components in the areas marked with ellipses and then executed an inverse Fourier transform, resulting in the target spectrogram shown in Fig. 3a. The details of the data processing using the bandpass filter are explained in Supplementary Note 3 with Supplementary Figs 2,3 and 4.

The delay-KER spectrogram retrieved from the target image in Fig. 3a is shown in Fig. 3b. The magnitude and phase of the retrieved a_v are also shown as solid circles with bars and as solid circles with connected lines in the bottom and middle panels of Fig. 4a, respectively. We have addressed the retrieval of the gate field in Supplementary Note 4 and show the magnitude and phase of the retrieved gate field in Supplementary Fig. 5. We also describe the performance and accuracy of the MW-FROG algorithm in ref. 9. According to the analysis in ref. 9, the large error in the retrieved magnitude is due to the bandpass filter. The phase error is sufficiently small to detect phase modulation with a magnitude of 0.2 rad, in spite of the bandpass filtering, by sequentially optimizing the complex amplitude of a_v and the polynomial expansion coefficients of the phase of a_v in the MW-FROG algorithm. The details of the optimization process are described in ref. 9. A non-trivial modulation, which cannot be compensated by arbitrarily adjusting the group delay (GD) offset of a wavepacket, appears in the retrieved phase in the middle panel of Fig. 4a. A similar phase modulation can also be observed in the retrieved data for the vibrational wavepacket of D_2^+, as shown in the middle panel of Fig. 4b.

Discussion

To clarify the origin of the phase modulation, we consider a theoretical model describing the transition amplitude of the ionization process[17,18]. In this model, the ionization process is described as a one-photon transition of a two-electron system, and the state of an ionized molecule is assumed to be a coherent superposition of the continuum electronic state accompanied by the $1s\sigma_g$ electronic state of a bounded electron in H_2^+. The details of this model is shown in Supplementary Note 5 with a timing chart of the pump and probe pulses depicted as Supplementary Fig. 6. Then, we apply the approximation that the electronic transition dipole matrix is fixed to that at the equilibrium distance of H_2. As a result, we can decompose the amplitude a_v into the product of $a_v^{\rm fc}$ and η_v, $a_v\propto a_v^{\rm fc}\eta_v$. The factor η_v is composed of the sum of the contributions from the ionization process induced by the nth harmonic component, η_v^n, namely,

$$\eta_v=\sum_{n=\rm odd}\eta_v^n, \tag{2}$$

where we define η_v^n as

$$\eta_v^n\equiv(\sigma_n^{\rm ion}/\omega_n^{\rm ph})^{1/2}\int_0^\infty {\rm d}\omega_{\rm e}\tilde{A}_n(\omega_{\rm e}-\omega_{\rm e}^{n,v}){\rm e}^{i\delta_1(\omega_{\rm e})}. \tag{3}$$

We denote the peak photon energy of the nth-order harmonic component as $\hbar\omega_n^{\rm ph}$ and the ionization cross section on irradiation of the nth-order component as $\sigma_n^{\rm ion}$ in equation (3). The amplitude $\tilde{A}_n(\Omega-\omega_n^{\rm ph})$ is the Fourier amplitude of the nth-order harmonic component, the peak magnitude of which

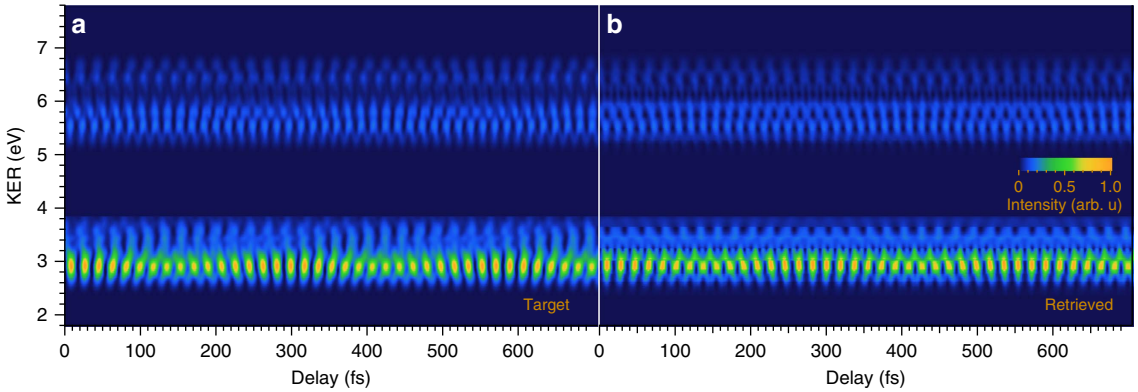

Figure 3 | Implementation of MW-FROG (**a**) Target delay-KER spectrogram used in the MW-FROG algorithm. (**b**) Retrieved delay-KER spectrogram. The target spectrogram in (**a**) is obtained from the experimental data in Fig. 2a using the bandpass filter. Details of the MW-FROG algorithm are given in ref. 9.

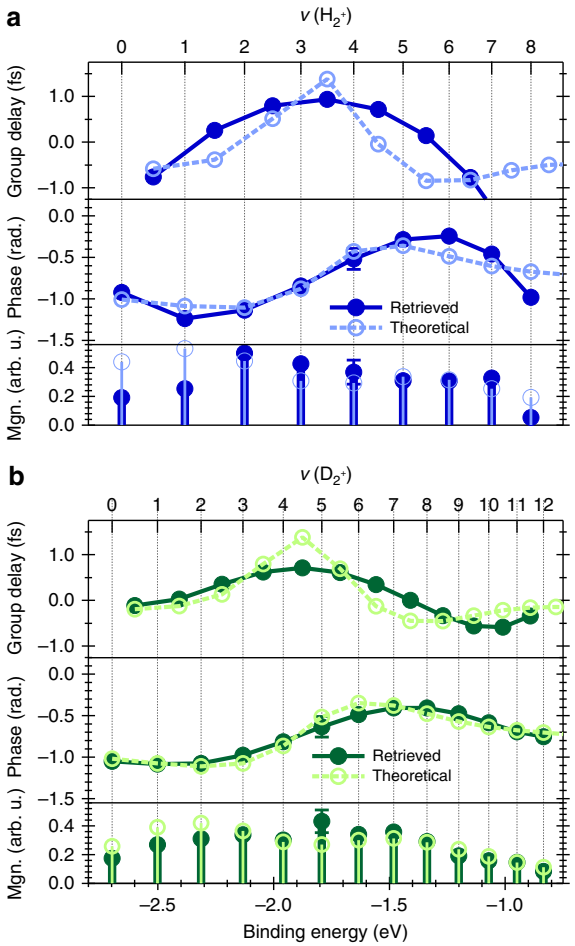

Figure 4 | Comparison of a_μ obtained with MW-FROG and the theoretical model. Magnitude (bottom panel), phase (middle panel) and GD (top panel) of vibrational wavepacket amplitudes for H_2^+ (**a**) and D_2^+ (**b**). Retrieved quantities are depicted as solid circles, while the data obtained from the theoretical model discussed in the text are shown as hollow circles. Error bars in magnitude and phase indicate root-mean-square errors in the relevant vibrational numbers, which were evaluated by the numerical test for MW-FROG algorithm reported in ref. 9. The GD is defined as the finite difference between adjacent phases. Thus, we plot GDs at the midpoints between adjacent vibrational quantum numbers. The binding energy is measured from the dissociation limit of H_2^+/D_2^+.

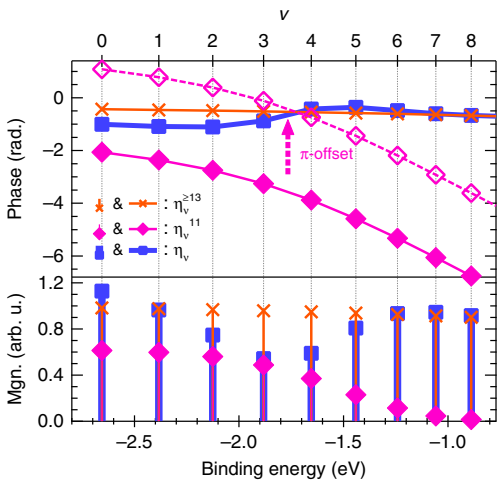

Figure 5 | Magnitude (bottom panel) and phase (top panel) of η_v for H_2^+ obtained from our model calculation The contribution from H13 to H21 ($\eta_v^{\geq 13}$) and that only from H11 (η_v^{11}) are shown as crosses and solid diamonds, respectively. Magnitude and phase of $\eta_v = \eta_v^{11} + \eta_v^{\geq 13}$ are depicted as solid squares in the bottom and top panels, respectively. We also show the phase of η_v^{11} with the π-offset, depicted as hollow diamonds, to clearly show the phase difference of π between η_v^{11} and $\eta_v^{\geq 13}$ at $v \sim 4$.

appears at $\Omega = \omega_n^{\rm ph}$. The continuum energy of the electron generated with the peak-energy photon of the nth-order harmonic component is denoted as $\omega_e^{n,v} \equiv \omega_n^{\rm ph} - \left(\omega_v^{\sigma_g} - \omega_0^X\right)$ The phase shift in the asymptotic form of the Coulomb wavefunction[19] of the ionized electron with an orbital angular momentum number of 1, $\delta_1(\omega_e)$, is included in equation (3). We neglect the contribution to the ionization from the continuum states with other orbital angular momenta[18]. The derivation of equations (2) and (3) is described in Supplementary Note 5.

As we state in Supplementary Note 5, the phase shift $\delta_1(\omega_e)$ does not exhibit a notable change in the continuum energy range of $\hbar\omega_e \gtrsim 2$ eV. Thus, we can recognize from equation (3) that the phase of η_v^n does not significantly differ with v when the harmonic order n is ≥ 13 because the photon energies of these orders of the harmonic field are all more than 2 eV larger than the energy of the dissociation limit and the variable ω_e to be integrated in equation (3) always lies in this range. This result is consistent with the constant phase of a_v obtained by assuming the conventional FC principle. We cannot expect, on the other hand,

the same trend for the phase of $\eta_v^{n=11}$, where the photon energy $\hbar\omega_{n=11}^{\rm ph}$ is close to $\hbar\omega_8^{\sigma_g} - \hbar\omega_0^X$, owing to the rapid change in $\delta_1(\omega_e)$ at $\omega_e \sim 0$.

The calculated results for $\eta_v^{\geq 13} \equiv \sum_{n=13}^{21} \eta_v^n$ and η_v^{11} are depicted in Fig. 5. We approximated $\widetilde{A}_n(\Omega)$ as the square root of the Gaussian fit to the measured high-harmonic spectra with a group delay dispersion (GDD) of $0.7 \times 10^{-32}\,s^2$ in this calculation. We explain how we estimated the GDD of the APT in Supplementary Note 5. The phases of a_v calculated with four different GDDs are also depicted in Supplementary Fig. 7. We found that the phase of $\eta_v^{\geq 13}$, depicted as crosses with connecting lines in the top panel of Fig. 5, decreases by only $\sim$0.2 rad when v is increased from 0 to 8. The phase of η_v^{11}, depicted as solid diamonds with connected lines, in contrast, decreases by more than 4 rad in the same range of vibrational quantum numbers. The significant feature of η_v^{11} is that the phase π-shifted from that of η_v^{11} intersects the phase of $\eta_v^{\geq 13}$ in the region of $3 < v < 4$, shown as hollow diamonds connected by dotted lines in the top panel of Fig. 5. This leads to destructive interference when we compute $\eta_v = \eta_v^{11} + \eta_v^{\geq 13}$.

We also show the calculated η_v in Fig. 5. The dip of $|\eta_v|$ around $v \simeq 3$, shown as solid squares with bars in the bottom panel of Fig. 5, is evidence of destructive interference due to the phase difference of π. The phase of η_v, depicted as solid squares with connecting lines in the top panel of Fig. 5, is also modulated for the same reason. The resultant magnitude and position of the phase modulation are in good agreement with the experimental data, shown as hollow circles with connecting dashed lines in the middle panel of Fig. 4a. The good agreement between the retrieved and calculated phases in D_2^+ is also exhibited in the middle panel of Fig. 4b. Hence, we conclude that we have observed a phase modulation of a_v caused by the interference between the continuum electron wavefunction emerging with the absorption of the 11th-order harmonic component and that emerging with the absorption of the higher-order components.

The phase of a wavefunction appearing in an ionization process is closely related to the time delay required for ionization, which can be measured by the attosecond streaking technique[20,21], two-colour high-order harmonic generation[22], or from the electron interference spectrogram obtained by using two-colour above-threshold ionization[23–26]. The phase of a_v in our study can also be interpreted as the time delay required for the formation of a vibrational wavepacket. We define the GD between the vth and $(v+1)$th vibrational states to be $\tau_v^{\rm GD} \equiv (arg\{a_{v+1}\} - arg\{a_v\})/(\omega_{v+1}^g - \omega_v^g)$, which should be a constant and exactly the same as the evolving time delay of the vibrational wavepacket if $arg\{a_v\}$ linearly increases with the binding energy. The GDs of a_v in H_2^+ obtained from the measured and modelled phases in our study both exhibit convex profiles in the region of $3 < v < 4$, as shown in the top panel of Fig. 4a. This characteristic is also revealed in the GDs of a_v in D_2^+ in the region of $4 < v < 5$, as shown in the top panel of Fig. 4b. According to these figures, the 3rd and 4th vibrational states in H_2^+ (4th and 5th vibrational states in D_2^+) are located $\sim$1 fs after the 1st and 2nd vibrational states in H_2^+ (in D_2^+). Therefore, we can state that delay of $\sim$1 fs is required to settle the initial vibrational states of $v = 0$–8 ($v = 0$–12) on the $1s\sigma_g$ state of H_2^+ (D_2^+) through the ionization process from H_2 (D_2) owing to the interference of the continuum electron.

We note that the above consideration of the settling time is only meaningful in the delay range in which the pump and probe pulses do not temporarily overlap, because we assumed this to derive equations (1), (2) and (3). We have addressed this issue in Supplementary Note 6. A more accurate description to conclude this study may be the following: the delay-KER spectrogram obtained by irradiation of the probe pulse after a sufficient delay ($\gtrsim$15 fs) is consistent with the physical model having an intrinsic $\sim$1-fs settling time difference of the vibrational states at the sudden emergence of the initial wavepacket, even though the initial wavepacket is actually prepared after passing through a $\sim$5 fs APT.

In spite of this limitation, our study has revealed a new physical insight into the birth of a vibrational wavepacket with a time scale of 1 fs. In particular, it is very important that the interference of the wavefunction of a continuum electron perturbs the motion of the nuclei, and thus, we can expect the possible control of the initial state of general nuclear motion through a coherent process in ionization. While the ionization time in the liberation motion of an electron is still an important observation to be measured in the attosecond scientific field, the settling time of the coherent motion of a large quantum system initiated via the ultrafast ionization of an electronic system should also be a new area of research to be investigated to solve the fundamental problems in the quantum time response of matter.

References

1. Feuerstein, B. *et al.* Complete characterization of molecular dynamics in ultrashort laser fields. *Phys. Rev. Lett.* **99,** 153002 (2007).
2. Calvert, C. R., Bryan, W. A., Newell, W. & Williams, I. D. Time-resolved studies of ultrafast wavepacket dynamics in hydrogen molecules. *Phys. Rep.* **491,** 1–28 (2010).
3. Kelkensberg, F. *et al.* Molecular dissociative ionization and wave-packet dynamics studied using two-color XUV and IR pump-probe spectroscopy. *Phys. Rev. Lett.* **103,** 123005 (2009).
4. Jiang, Y. H. *et al.* Investigating two-photon double ionization of D_2 by XUV-pump–XUV-probe experiments. *Phys. Rev. A* **81,** 051402(R) (2010).
5. Thumm, U., Niederhausen, T. & Feuerstein, B. Time-series analysis of vibrational nuclear wave-packet dynamics in D_2^+. *Phys. Rev. A* **77,** 063401 (2008).
6. Jiang, Y. H. *et al.* Tracing direct and sequential two-photon double ionization of D_2 in femtosecond extreme-ultraviolet laser pulses. *Phys. Rev. A* **81,** 021401(R) (2010).
7. Urbain, X. *et al.* Intense-laser-field ionization of molecular hydrogen in the tunneling regime and its effect on the vibrational excitation of H_2^+. *Phys. Rev. Lett.* **92,** 163004 (2004).
8. Trebino, R. *et al.* Measuring ultrashort laser pulses in the time-frequency domain using frequency- resolved optical gating. *Rev. Sci. Instrum.* **68,** 3277–3295 (1997).
9. Nabekawa, Y. *et al.* Frequency-resolved optical gating technique for retrieving the amplitude of a vibrational wavepacket. *Sci. Rep.* **5,** 11366 (2015).
10. Nabekawa, Y. *et al.* Conclusive evidence of an attosecond pulse train observed with the mode-resolved autocorrelation technique. *Phys. Rev. Lett.* **96,** 083901 (2006).
11. Nabekawa, Y. *et al.* Interferometric autocorrelation of an attosecond pulse train in the single-cycle regime. *Phys. Rev. Lett.* **97,** 153904 (2006).
12. Furukawa, Y. *et al.* Nonlinear Fourier-transform spectroscopy of D_2 using high-order harmonic radiation. *Phys. Rev. A* **82,** 013421 (2010).
13. Furukawa, Y. *et al.* Resolving vibrational wave-packet dynamics of D_2^+ using multicolor probe pulses. *Opt. Lett.* **37,** 2922–2924 (2012).
14. He, F. & Thumm, U. Dissociative ionization of H_2 in an attosecond pulse train and delayed laser pulse. *Phys. Rev. A* **81,** 053413 (2010).
15. Fábri, C., Czakó, G., Tasi, G. & Császár, A. G. Adiabatic Jacobi corrections on the vibrational energy levels of H_2^+ isotopologues. *J. Chem. Phys.* **130,** 134314 (2009).
16. Kulander, K. C., Mies, F. H. & Schafer, K. J. Model for studies of laser-induced nonlinear processes in molecules. *Phys. Rev. A* **53,** 2562–2570 (1996).
17. O'Neil, S. V. & Reinhardt, W. P. Photoionization of molecular hydrogen. *J. Chem. Phys.* **69,** 2126–2142 (1978).
18. Itikawa, Y., Takagi, H., Nakamura, H. & Sato, H. Theoretical studies of photoionization of hydrogen molecules. *Phys. Rev. A* **27,** 1319–1327 (1983).
19. Serov, V. V., Derbov, V. L. & Sergeeva, T. A. Interpretation of time delay in the ionization of two-center systems. *Phys. Rev. A* **87,** 063414 (2013).
20. Cavalieri, A. L. *et al.* Attosecond spectroscopy in condensed matter. *Nature* **449,** 1029–1032 (2007).
21. Schultze, M. *et al.* Delay in photoemission. *Science* **328,** 1658–1662 (2010).
22. Shafir, D. *et al.* Resolving the time when an electron exits a tunnelling barrier. *Nature* **485,** 343–346 (2012).
23. Månsson, E. P. *et al.* Double ionization probed on the attosecond timescale. *Nat. Phys.* **10,** 207–211 (2014).
24. Klünder, K. *et al.* Probing single-photon ionization on the attosecond time scale. *Phys. Rev. Lett.* **106,** 143002 (2011).

25. Caillat, J. *et al.* Attosecond resolved electron release in two-color near-threshold photoionization of N_2. *Phys. Rev. Lett.* **106,** 093002 (2011).
26. Kelkensberg, F. *et al.* Attosecond control in photoionization of hydrogen molecules. *Phys. Rev. Lett.* **107,** 043002 (2011).

Acknowledgements

We thank Professor Shuntaro Watanabe and Professor Jiro Itatani for providing us with the technical information concerning a piezo gas valve used to supply target molecules to the VMI chamber. This work was part of the Advanced Photon Science Alliance (APSA) research project, commissioned by MEXT of Japan. Y.N., T.O, E.J.T, and K.M. gratefully acknowledge financial support from Grants-in-Aid for Scientific Research Nos. 26247068, 26600123, 25286074, 26600122 and 26220606.

Author contributions

Y.N. developed the laser system, conceived the MW-FROG measurement of a vibrational wavepacket, gave the theoretical model for the measured phase, and wrote the manuscript. Y.F. was responsible for the data acquisition and analysis required to obtain the delay-KER spectrogram. T.O. designed and built the VMI spectrometer and developed the data acquisition software. A.A.E. was also involved in the development of the laser system. E.J.T developed the high-harmonic beam line and XUV spectrograph. K.Y. supervised the experiment on VMI. K.M. directed the research in accordance with the Extreme Photonics research project of RIKEN and the APSA research project of MEXT.

Additional information

Supplementary Information accompanies this paper at http://www.nature.com/naturecommunications

Competing financial interests: The authors declare no competing financial interests.

Reprints and permission information is available online at http://npg.nature.com/reprintsandpermissions/

How to cite this article: Nabekawa, Y. *et al.* Settling time of a vibrational wavepacket in ionization. *Nat. Commun.* 6:8197 doi: 10.1038/ncomms9197 (2015).